Overview of electrical power models for concentrated photovoltaic systems

P. Voarino, Mousaab Benhammane, Gilles Notton, Grégoire Pichenot, Yannick Roujol, F. Chabuel

Overview of electrical power models for Concentrated Photovoltaic systems and development of a new operational model with easily accessible inputs

Mousaab Benhammane[1,2], Gilles Notton[2,*], Grégoire Pichenot[3], Philippe Voarino[1], David Ouvrard[2]

[1]Département des Technologies Solaires - Laboratoire Modules Photovoltaïques Intégrés - CEA, LITEN, INES. 50 avenue du Lac Léman - F-73375 Le Bourget-du-Lac - France

[2]Université de Corse – UMR CNRS 6134 – Centre Scientifique Georges Péri – Route des Sanguinaires – F20000 Ajaccio – France

[3]Département des Technologies Solaires - Laboratoire des Systèmes Electriques Intelligents - CEA, LITEN, DTS, INES. 50 avenue du Lac Léman - F-73375 Le Bourget-du-Lac - France

Abstract: The utilization of multi-junction solar cells with high efficiency is still not widespread for terrestrial power applications. These solar cells, composed by several material layers, reach high efficiencies but its cost is expensive, more of 100 higher than classical silicon solar cells. Thus, one solution consists to use reduced sizing solar cells associated with optics mounted on solar tracker to concentrate the solar beam. Numerous meteorological parameters such as beam solar irradiance, ambient temperature and air mass and especially spectral characteristics of sun radiation are involved in the conversion process and are generally used as inputs in power models. Several models from literature, different by their form and by the number and type of input variables, are presented; based on this state-of-art, some similar models are selected and tested on two experimental CPV systems located on two different sites, Ajaccio and Le Bourget du Lac. Then, an operational model of electrical power using inputs easily measured and available for a solar CPV plant operator is developed. It could be used as a decision-aided tool for investors in providing an estimation of the energy production capacity of the CPV systems on the future implantation site. This established model based on data measured on the CPV system in Ajaccio estimates the produced power with a root mean square error of about 5% on the two sites using only a reduced number of inputs.

Keywords: Concentrator Photovoltaics systems; Multi-junction solar cells; Operational Model; Experimentation; Electrical power estimation.

---

* Corresponding author : notton_g@univ-corse.fr

Introduction

The Planar photovoltaic (PV) system is today a proven technology and its share of the energy supply in the planet is increasing substantially, exceeding the original growth forecasts. Energy supplying becomes today the biggest concerns for developed and developing countries due to the growing energy needs in the last decades and the utilization of Renewable energy will contribute greatly to the energy production in increasing the energy autonomy of countries [1].

At the end of 2018, the photovoltaic capacity exceeded half a million Megawatts, which equates to about 100 GWp of newly installed capacity. In 2018, China's market faltered, while there was a revival in the European Union market and the emerging markets picked up steam. The growth of the market of photovoltaic energy systems over these last years is always continuing. A PV capacity of 7.6 GWp was installed in 2018 in Europe, 44.4 GWp in China, 10.6 GWp in USA, 10.8 GWp in India, 6.5 GWp in Japan, 2 GW in South Korea, 1.6 GWp in Turkey, 3.8 GWp in Australia and 2.7 GWp in Mexico. Thus, the total capacity respectively in Europe and globally reached 114.85 GWp and 480.36 GW for PV [2-3] at the end of 2018.

One of the criticisms made of these PV systems is their low density of production mainly due to the low power density and intermittence of the solar resource and to the limited efficiency of the photovoltaic conversion. To address this low efficiency, numerous researches were conducted on new PV cells technologies such as multi-junction solar cells (MJSC) reaching high efficiencies exceeding 30% [4] without any light concentration. The cost of these cells being very high, more than 100x than classical silicon solar cells, the material quantity must be reduced. Thus, small cells are associated with optics (mirrors and low cost lenses) to concentrate the beam solar radiation; the utilization of a concentrating device implies the use of solar tracker affecting the reliability, increasing the complexity and the cost of such Concentrators Photovoltaics (CPV) systems.

CPV technology entered the market in the 1980's as a utility scale solar power generation option. More than 90% of the capacity installed until 2015 is based on high concentration PV (HCPV) with two-axis trackers (300x to 1000x) onto a small MJSC based on III-V semiconductors. Most of them are lattice-matched solar cells made of GaInP, GaInAs and Ge [4].

Compared to conventional PV, the CPV market is still small, with a market volume around 70 MWp in 2014. For 2015 a total number of new installations between 10 and 25 MWp is estimated and a total installed CPV system (>1MWp) of about 300GWp of CPV at the end of 2015. The CPV industry has witnessed turbulent times with the number of new installations significantly declining in 2015 as compared to the past [5]. The CPV market generated approximately USD 790 million in 2014 [6], and its size is predicted to exhibit about 14% CAGR from 2016 to 2024. It would reach a size of nearly USD 2.1 billion by 2024 [7].

If the modelling of a "conventional" PV modules behaviour was considerably studied in the literature, the modelling of CPV systems is relatively unexplored. This modelling is more difficult because

conversion process is more complicated and inputs more numerous: beam solar irradiance, ambient temperature and wind speed but also the spectral decomposition of the sun radiation depending on the atmosphere state and thickness. The spectral composition of the sun radiation is poorly measured and available for CPV plant operators.

The paper will have the following structure:

- the first paragraph presents the various electrical power models used for CPV systems;
- the second one describes the two CPV experimentations used for the validation of the models;
- from this literature review, some structures of power models are selected and their performances are performed in a third paragraph;
- at last, an operational model is developed, based only on easily available measured data for CPV operators and validated on two experimental sites.

1. Literature reviews of multi-junction CPV power models

This state-of-art of electrical power models for HCPV systems presented here will provide a basis for the choice of some models which will be validated in the paragraphs 3 and 4. The objective is to sort the theoretical models thanks to inputs that will be easily extractable from the experimental monitoring of CPV plants. At the end, one of them will be selected and more specifically studied. Only Direct Current (DC) models are expressed by considering that CPV systems operates in maximum power point (MPP) conditions.

1.1. Equivalent circuit of a multi-junction cells

Two equivalent-circuit approaches are used: a 1-diode and a 2-diode model; and an equivalent circuit represents each sub-cell of the MJSC. The MJSC voltage V is equal to the sum of the sub-cell voltages V_i, where i defines the sub cell i. The photo-generated current $I_{ph,i}$ of a sub-cell or I_{ph} of the MJSC are considered as equal to the respective short-circuit currents $I_{sc,i}$ and I_{sc}, the diode current being considered as negligible [8]. The 1D and 2D models are:

$$I_i = I_{sc,i} - I_{0,i} \left(e^{\frac{q \cdot (V_i + I \cdot R_{S,i})}{n_i \cdot k_B \cdot T_{cell}}} - 1 \right) - \frac{(V_i + I \cdot R_{S,i})}{R_{sh,i}} \tag{1}$$

$$I_i = I_{sc,i} - I_{01,i} \left(e^{\frac{q \cdot (V_i + I \cdot R_{S,i})}{n_{1i} \cdot k_B \cdot T_{cell}}} - 1 \right) - I_{02,i} \left(e^{\frac{q \cdot (V_i + I \cdot R_{S,i})}{n_{2i} \cdot k_B \cdot T_{cell}}} - 1 \right) - \frac{(V_i + I \cdot R_{S,i})}{R_{sh,i}} \tag{2}$$

In the 2D model, two modes of losses, radiation and non-radiation recombination, are presented. I_0, I_{01} and I_{02} are the saturation current of the diodes. $R_{S,i}$ and $R_{sh,i}$ are the serial and shunt resistances of the sub-cell i. T_{cell} is the cell temperature in Kelvin. The 1D model has five parameters ($I_{sc\ i}$, I_0, n_i, $R_{S,i}$ and $R_{sh,i}$) and the 2D model has seven parameters ($I_{sc,i}$, I_{01}, I_{02}, n_{i1}, n_{i2}, $R_{S,i}$ and $R_{sh,\ i}$).

Fernández et al. [9] compared different methods to determine these parameters from I-V measures under various irradiance and temperature conditions. Other methods were described by Segev et al.

3

[10], Nishioka et al. [11-12] and Or and Appelbaum [13] for the 2D model. Generally, these parameters are determined under controlled conditions.

1.2. Dominguez'model (2010)

The Domínguez'model [14] is based on the 1D model but the three resistances $R_{S,i}$ are replaced by one effective one R_S. The effect of the shunt resistance is neglected. The method consists in translating the I-V curve for different conditions of spectra, concentration and temperature. The estimation of I-V curves is obtained with a Root Mean Square Error (RMSE) between 0.53% and 0.85% for T_{cell} between 25°C and 75°C for concentration between 100 and 700 suns.

1.3. Fernández'model (2013)

The Fernández'model [15-16] is also based on a 1D model of a three-junction cell (GaInP/GaInAs/Ge). The cell current is only limited by the two upper sub-cells GaInP and GaInAs respectively called « Top » and « Middle ». Actually, Ge sub-cell called « Bottom » absorbs a large spectral band in the infrared part of the solar spectrum and then produces an excess of current. Then only « Top » and « Middle » sub-cells are taken into account in the 1D model. The experiments were realized for cell temperature T_{cell} = 10°C, 45°C, 75°C and 100°C with a variation of the solar spectrum (the spectral matching ratio between the « Top » and « Middle » subcells varied between 0.78 and 1.22). The relative Mean Bias Error (MBE) for the estimation of I-V curve was 0.16%. The inconvenient of this method is the necessity to measure the External Quantum Efficiency (EQE) of the two sub-cells, the I-V curve and a spectral ratio to determine the model coefficients; moreover, this model can be applied only to a lattice matched GaInP/GaInAs/Ge solar cell.

1.4. Syracuse model (2005)

The Syracuse model developed by Ekins-Daukes et al [17] is based on a 2D-model. The photo-generated model is estimated from the beam solar irradiance for a given wavelength of the Direct Normal Irradiance (DNI_λ) calculated using the SMARTS software. SMARTS2 [18] is a free tool available since 1995 and developed by Gueymard in NREL which is an alternative to a solar spectrum measure. SMART uses an atmospheric radiation transfer model to generate a solar spectrum under clear sky conditions for a given site from meteorological data such as Air Mass (AM) and Atmospheric Optical Depth (AOD) and Precipitable Water (PW).

This approach was used by Chan et al. [19] to model the electrical power of 3J high CPV modules in Japan using spectral data obtained with SMARTS and AOD values given by AERONET [20] and PW values computed from air temperature T_{air} and relative humidity RH [19].

The EQE is used to determine the photo-generated current of the sub-cells [21] taking into account the variation of the gap energy for each semiconductor material with temperature according to the Varshni formulation [19]. The annual produced energy by the HCPV system was estimated with an error of about 2%. This model allows to have a detailed knowledge of the 3J cell behaviour but its

application is limited because it needs to have the measures under various conditions of T_{cell}, I-V curves and EQE.

1.5. Yield Opt model (2015)

Steiner et al [21-22] developed the « Yield Opt » model considered as a more complex version of the Syracuse model. It uses also the SMARTS tool to determine the solar spectrum and integrates a model to define the optical spectral transmission Tr_{optic} for a lens temperature T_{lens} given by a ray tracing software and a finite elements calculation, to get the shape deformation of the Primary Optical Element (POE) for a given T_{lens}. The electrical power, obtained from IV curves, is corrected by a tracking misalignment correction coefficient ε taking into account the power loss induced by a given misalignment of the tracker.

Steiner et al [21-22] calculated a good RMSE between 2.6% and 3.9% for calculating the electrical power of various HCPV modules. But, this model is complex and need to know the misalignment measure and a fine knowledge of the cell and optical processes.

1.6. Kinsey model (2008)

Kinsey et al [23-24] proposed a model based on a 1D representation. They calculated the MPP power P_{mpp} from the short-circuit current density J_{sc}, the cell surface A_{cell}, the open-circuit voltage V_{oc} and the fill factor FF by [23-24]:

$$P_{mpp} = J_{sc} \cdot A_{cell} \cdot V_{oc} \cdot FF \qquad (3)$$

J_{sc} is calculated from isotype cell measures, EQE and the solar spectrum. FF and V_{oc} are determined from the value under standard conditions corrected by the temperature effect. This model needs the measure of EQE for various T_{cell}, I-V curves and solar spectrum. A difference of 2% was obtained between the energy calculated by the Kinsey model and measured [25].

1.7. Peharz model (2011)

Peharz et al. [26] developed a model using the parameter Z, the beam solar irradiance DNI and the cell temperature T_{cell} :

$$P_{mpp} = c_{DNI} \cdot DNI + c_{Z2} \cdot Z^2 + c_Z \cdot Z + c_{T_{cell}} \cdot T_{cell} + c_{offset} \qquad (4)$$

The coefficients c_{DNI}, c_{Z2}, c_Z, c_{Tcell} and c_{offset} are obtained by linear regression from experimental data in real condition of operation. The parameter Z was introduced by Meusel et al [27]. It indicates the current imbalance of two sub-cells under a given solar spectrum compared to a solar spectrum AM1.5D. Z = 0 for a spectrum identical to AM1.5D, Z > 0 or Z < 0 if the solar spectrum is bluer or redder for a 3J cell. The calculation of Z is given by Peharz et al [28]. In equation (4):

- $c_{DNI} \cdot DNI$ traduces the linearity between the power and the beam solar irradiance at constant temperature and spectrum.
- $c_{T_{cell}} \cdot T_{cell}$ expresses the power variation with T_{cell}.
- $c_{Z2} \cdot Z^2 + c_Z \cdot Z$: according to the HCPV module, Peharz et al. [27] approximates the variation of the power versus Z by a straight line $(c_Z \cdot Z)$ or by a 2nd degree polynomial expression $(+c_{Z2} \cdot Z^2)$.
- c_{offset} : a constant to take into account a threshold effect or a misalignment.

Peharz et al. [26] applied this model on four different HCPV modules in Freiburg (Germany) and obtained a RMSE of 1.3W, 1.2W, 1.6W and 0.6W for PV modules with a power under Concentrator Standard Test Conditions (CSTC) of 54W, 50.1W, 44W and 15.7W. The main disadvantages of this method are:
- the estimated power is non-zero at DNI = 0 W.m-2,
- component solar cells or isotypes must be used for Z calculation,
- this method was also used to calculate the power under Concentrator Standard Operating Conditions (CSOC) with a RMSE between 2% and 4%.

1.8. SANDIA model (2004)

The model developed in SANDIA Laboratory [29] by Kratochvil et al known also under the name "photovoltaic array performance model" is based on CPV experiments under real solar irradiance. It considers the influence of the solar spectrum via a spectral correction factor depending only on the Air Mass in introducing an effective irradiance DNI_{eff}. This factor was introduced by the ASTM E 973 Standard and approximated by a 4th degree polynomial expression [29] (Equation (5)).

$$f_1(AM) = a_0 + a_1 AM + a_2 AM^2 + a_3 AM^3 + a_4 AM^4 \qquad (5)$$

$$DNI_{eff} = \frac{DNI}{DNI_{réf}} f_1(AM) \qquad (6)$$

The IV curve is calculated from five operating points (which are $[I_{sc}, 0]$, $[I_{Voc/2}, V_{oc}/2]$, $[I_{mpp}, V_{mpp}]$, $[(I_{sc} + I_{mpp})/2, (V_{oc} + V_{mpp})/2]$, $[0, V_{oc}]$) the MPP current is function of DNI_{eff} and T_{cell} :

$$I_{mpp} = (C_0 \, DNI_{eff} + C_1 \, DNI_{eff}^2)\left(I_{mpp,ref} + \alpha_{I_{mpp}} \cdot (T_{cell} - T_{cell,ref})\right) \qquad (7)$$

$\alpha_{I_{mpp}}$ is a coefficient traducing the variation of the MPP current with temperature.

V_{mpp} is expressed versus the logarithm of DNI_{eff}; $\beta_{V_{mpp}}$ is a coefficient traducing the variation of the MPP voltage with temperature [30]:

$$V_{mpp} = V_{mpp,ref} + C_2\,N_s\,\frac{n\,k_B T_{cell}\,\ln(DNI_{eff})}{q} + C_3 N_s \left(\frac{n\,k_B T_{cell}\,\ln(DNI_{eff})}{q}\right)^2$$
$$+ \beta_{V_{mpp}}\left(T_{cell} - T_{cell,ref}\right) \tag{8}$$

C_0, C_1, C_2 and C_3 are obtained by linear regression from measured data.

This model has for advantages to have its coefficients calculated from experimental data in real conditions, but it is necessary to know the values of some intrinsic parameters of the PV module such as n, N_s and the law between DNI and AM (Eq.(5)). This model tested on a HCPV system in Jaén in Spain [30] calculates the power with a RMSE equal to 3.4%.

1.9. Model used in PVSyst software

PVSyst [31] is a commercial software for the sizing and the production estimation for various PV modules and plants. Soitec, a HCPV module suppliers, collaborated with PVSyst to develop a power model for the CX–M500 module (3J cells under a concentration of 500 suns, 2.45 kWc). The PVSyst approach [32] consists in realizing IV curves measured under real illuminations for various irradiances and temperature and to determine the parameters of the 1D model. An Utilization Factor (UF) was introduced, sum of three linear functions depending on DNI, T_{air} and AM [32]. This model, validated on IV curves during one and a half year in Seville, Spain, estimates the HCP power with a RMSE of 3.7% and a MBE of -0.8% [32]. It was also tested on four HCPV plants in Middle East and South Africa, the RMSE and MBE values are given in Table1.

Table 1. RMSE and MBE values for the estimation of HCPV power by PVSyst.

Sites	Power installed (kWp)	MBE (%)	RMSE (%)
Sede Boqer, Israel	6	0.7	10.7
Touwsrivier, South Africa	44000	- 0.6	12.5
Shams Ma An, Jordan	10	1.7	9.0
Muscat, Oman	6	- 4.2	8.7

PVSyst is a tool to calculate the energy produced and not the HCPV power, from meteorological data characteristic of the site. We can underline that the three functions for the UF determination describe independent phenomena, inducing some difficulties to determine the coefficients [33]. Furthermore, this approach would need according to PVSyst developers the knowledge of the module via long-term measures [34].

1.10.   Standard ASTM E 2527-09

The standard ASTM E 2527-09 [35] is the only "official" formulation to calculate the CPV power under real operating conditions from DNI, T_{air} and v (wind speed):

$$P_{mpp} = DNI\,(a_1 + a_2\,.\,DNI + a_3\,.\,T_{air} + a_4\,.\,v_{vent}) \tag{9}$$

a_1, a_2, a_3 and a_4 are deduced by linear regression from experimental data under real conditions, no variable depending on the solar spectrum are used. A filter criterion defined by the standard ASTM E 2527-06 [36] is applied to the experimental data. Rodrigo et al. [30] tested this model on two HCPV modules located at Jaén in Spain during two years and found a RMSE equal to 4.6%.

1.11. Garcia-Domingo model (2014)

García-Domingo et al. [37] developed a power model using as input DNI, T_{air}, v and the spectral matching ratio $SMR_{\frac{Top}{Middle}}$ defined as the ratio of two short-circuit current density [38]:

$$SMR_{\frac{Top}{Middle}} = \frac{\left(J_{sc,Top}/J_{sc,Top,ref}\right)}{\left(J_{sc,Middle}/J_{sc,Middle,ref}\right)} \tag{10}$$

The Spectral Factor SF was expressed versus $SMR_{\frac{Top}{Middle}}$ and introduced in the formulation of the HCPV power. From data of Jaén, Spain, Garcia-Domingo et al [37] validated their model with a RMSE=5.3%.

Note that this method has the advantage to take into account the variation of the solar spectrum but a measure using component solar cells is needed which complicates this method.

1.12. Garcia-Domingo model based on Standard ASTM E 2527-09 (2015)

García-Domingo et al. [39] modified the ASTM E 2527-09 model [35] in adding a spectral variable APE (Average Photon Energy). APE is aiming to the characterization of the energetic distribution in an irradiance spectrum. It is obtained by dividing the irradiance by the photon flux density [40-41] and it allows to evaluate the impact of a variation of the solar spectrum for various technologies particularly studied by Moreno Sáez et al. [42], Ishii et al. [43], Piliougine et al. [44], Nofuentes et al. [45] and Cornaro et al. [46]. The effect of APE on the CPV performances was studied by Gueymard et al. [47] and Husna et al. [48]. The CPV power is calculated by Eq (11), a_1, a_2, a_3, a_4 and a_5 depend on the interval of APE.

$$P_{mpp} = DNI\,(a_1 + a_2\,.\,DNI + a_3\,.\,T_{air} + a_4\,.\,v + a_5\,.\,APE) \tag{11}$$

From data measured on 2 HCPV modules in Jaén, the Mean Absolute Error (MAE) obtained by this model was between 1.9% and 3.9% [39].

1.13. Fernandez Models (2013-2015)

Fernandez et al [49] developed three models in which the cell temperature is calculated from DNI and T_{air} by the Almonacid formula [50]. The three models are:

$$P_{mpp} = \frac{P_{mpp,ref}}{DNI_{ref}} \cdot DNI \cdot \left(1 - \delta\left(T_{cell} - T_{cell,ref}\right)\right) \tag{12}$$

$$P_{mpp} = \frac{P_{mpp,ref}}{DNI_{ref}} \cdot DNI \cdot \left(1 - \delta\left(T_{cell} - T_{cell,ref}\right)\right) \cdot \left(1 - \varepsilon(AM - AM_u)\right) \tag{13}$$

$$P_{mpp} = \frac{P_{mpp,ref}}{DNI_{ref}} \cdot DNI \cdot \left(1 - \delta\left(T_{cell} - T_{cell,ref}\right)\right) \cdot \left(1 - \varepsilon(AM - AM_u)\right) \cdot \left(1 - \varphi\left(AOD_{550} - AOD_{550,u}\right)\right) \tag{14}$$

$P_{mpp,ref}$ is the PV power for DNI, T_{cell}, AM and AOD_{550} equal respectively to DNI_{ref}, $T_{cell,ref}$, AM_u and $AOD_{550,u}$. AM_u and AOD_u are the values of AM and AOD for which the PV power is maximum. The coefficients δ, ε and φ are obtained by linear regression from measured data. AOD_{550} values are obtained at a daily scale from MODIS website of NASA [51].

These models were tested on the Jaen Site in Spain and the results are given in Table 2.

Table 2. Performance metrics for the three Fernandez models

	RMSE (%)	MAE (W)	MBE (%)	R²
Equation (12)	5.0	7.5	0.4	0.92
Equation (13)	3.5	5.6	-0.3	0.98
Equation (14)	2.7	4.2	0.2	0.99

These models have some advantages: easy to implement, the T_{cell} model has been validated under real conditions, but also some disadvantages: necessity to measure T_{cell} (difficult for CPV modules) and AOD is not available for all the sites.

Fernandez et al [52] proposed an optimised version of the second model by replacing T_{cell} by T_{air} (with $T_{air,ref}$ being equal to 20°C):

$$P_{mpp} = \frac{P_{mpp,ref}}{DNI_{ref}} \cdot DNI \cdot \left(1 - \delta\left(T_{air} - T_{air,ref}\right)\right) \cdot \left(1 - \varepsilon(AM - AM_u)\right) \tag{15}$$

Fernandez et al [52] studied the influence of AM on the electrical power for two CPV modules in Jaen, it appears that this influence is negligible for AM ≤ 2 and then a simplified version without AM is used for this range. This model was tested on two years of data and a RMSE equal to 3.5% was obtained.

1.14. Artificial Neural Network approach

Some approaches based on Artificial Neural Network (ANN) approach were used to model the IV curve of CPV modules. Almonacid et al [53] tested this model which gives good results hardly generalizable and needing a large data set for the training, not easily available.

1.15. Synthesis of the sixteen CPV models

Table 3 presents a synthesis of the variables used in each of the sixteen models located in the first column of the table. These models created from 2004 to 2016 are relatively new. They have between two and seven inputs (see from 2nd to 14th column). All models have as input the direct normal irradiance DNI. The temperature (air, cell, module) and the spectrum (AOD, AM, Isc, EQE, transmission) are other relevant parameters. The wind and tracker effect parameters are not often used. We can distinguish, based on the output of the models, two groups: I-V curve modelling (15th column) and P_{mpp} modelling approaches (16th column). Approaches of the first category helps more understanding of the module operation, however they would need to be used a detailed knowledge of the module, which is not the case for the P_{mpp} models. The parameters of these ones, however, would need to be fitted a sufficient period of measurement.

Some models were tested and validated on data measured at Jaen, Spain and showed a RMSE value between 2.7% and 5.3%. Other models were evaluated in terms of MAE (Mean Absolute Error) with a value between 1.9% and 7.5%. These values of RMSE and MAE can be used as a reference but it is necessary to keep in mind that the validation was realized on various systems, installed in various sites with different meteorological conditions. Thus carrying out a study of theoretical models on two other sites with distinct characteristics will complete this state of the art. In addition, it will be more relevant to sort out the efficiency of the same models on several production sites.

Table 3. Synthesis of input and output data for the sixteen CPV models.

| Model | Input | | | | | | | | | | | | | Output | |
	DNI	Solar spectrum	T_{air}	T_{cell}	T_{lens}	v	PW	AOD	AM	$I_{sc,i}/I_{sc}$	EQE	$T_{r,opt}$	ε	I-V curve	P_{mpp}
Equivalent circuit	√	√		√			√	√	√	√	√			√	
Dominguez (2010)	√			√						√				√	
Fernandez (2013)	√			√						√				√	
SANDIA (2004)	√			√					√						√
Syracuse (2005)	√	√		√			√	√	√	√	√			√	
Yield Opt (2015)	√	√		√	√		√	√	√	√	√	√	√	√	
Kinsey (2008)	√	√		√						√	√				√
Peharz (2011)	√			√						√					√
PVSyst (2010)	√		√						√					√	
ASTM (2006)	√		√			√									√
Garcia Domingo (2014)	√		√							√					√
Garcia Domingo (2015)	√	√	√			√				√					√
Fernandez1 (2013)	√		√	√											√
Fernandez2 (2013)	√		√	√					√						√
Fernandez3 (2013)	√		√	√					√						√
Fernandez4 (2015)	√		√						√						√

The main difficulty in some presented models is the utilization of meteorological data difficult to obtain for the studied site as AOD and PW mainly with a relatively small time step (the variation of these parameters over the year and over the day can be important) or complex to calculate as EQE, I_{sci}/I_{sc}, $T_{r,opt}$ and the solar spectrum. Our objective being to develop a model easy to implement and requiring easily available inputs in view to be operational and usable by PV system developers, the influence of these less available parameters on the quality of the produced PV power at the beginning of paragraph 2.must be estimated.

2. Presentation of the two experimentations

In this paragraph, the two experimental CPV systems located in Le Bourget du Lac and in Ajaccio and the measuring systems are presented.

The objectives of the presentation are to show the similarities of the CPV systems (excepted for the tracking method) and the differences between the two sites from a meteorological point of view which influences the spectral quality of the solar radiation important in multi-junction cells operation.

Moreover, a specific attention will be given to the quality check and pre-treatment of the meteorological and electrical data.

2.1. The CPV systems

Two CPV systems were used to validate the power model: the first one was installed in Bourget du Lac in Savoie and the second one in Ajaccio, Corsica (Figure 1).

Figure 1. Position of the experimental sites and overview of the two sites.

Le Bourget du Lac

A CPV system was installed by the manufacturer of solar tracker Helioslite running with one motor [54] on the research site of INES (Institut National d'Energie Solaire) on June 2017. It is composed by 64 modules of 87.5 Wp i.e. 5.6 kWp connected to an inverter of 6 kW (Figure 2). The HCPV module SM-U01 was built by Semprius and is composed of micro-concentrators with a concentration ratio

equal to 1111 suns and of three junction micro-cells in GaInP/GaInAs/GaInNAs with an area < 1mm². The main characteristics are given in Tables 4 and 5.

Figure 2. CPV system installed in Le Bourget du Lac.

Table 4. Description of the CPV module (Semprius SM-U01)

CPV module characteristics					
Cell			**Primary Optical Element (POE)**		**Secondary Optical Element (SOE)**
Type	Cell efficiency	Size (mm x mm)	Type	Size (mm x mm)	
3 J cells (GaInP/GaInAs/GaInNAs)	41% (CSTC)	0.6 x 0.6	Plano-convex lens in silicone on glass (SOG)	20 x 20	Spherical balls in glass
Sizes (length x width x thickness) 636 mm x 476 mm x 66 mm			**Number of cells** 660 cells (22 chains of 30 cells connected in serial)		

Table 5. Electrical characteristics of the CPV module (Semprius SM-U01)

CPV module electrical performances											
Under controlled illumination (CSTC)						**Under real illumination (CSOC)**					
P_{mpp} (W)	V_{mpp} (V)	I_{mpp} (A)	V_{oc} (V)	I_{sc} (A)	Efficiency (%)	P_{mpp} (W)	V_{mpp} (V)	I_{mpp} (A)	V_{oc} (V)	I_{sc} (A)	Efficiency (%)
87.5 (± 5%)	86.6	1.01	101.6	1.06	33.9	70 W	81	0.86	95	0.9	31.2

The measuring system is composed from:

- a pyrheliometer Kipp & Zonen SHP1-A mounted on a 2AP sun tracker measuring DNI;

- a spectro-pyrhéliometer (Solar Added Value) measuring the three short circuit currents for each sub-cell with a spectral band between 370 nm and 1650 nm;

- a solar spectral sensor SolarSIM-D2 (Spectrafy[TM]) D2 using silicon photodiodes integrated with band pass interference filters to monitor discrete sections of the solar spectrum (280 nm-4000 nm);

- a meteorological station Vaisala WTX520 measuring the air temperature, the wind speed and direction, the relative humidity and the atmospheric pressure;
- the currents of the two trackers are measured in order to adjust the tracking angle.

Ajaccio

The HCPV system of 112 modules Semprius SM-U01 was installed by Helioslite on the R&D platform in the University of Corsica. This system is working since April 2016; the total CPV power is 9.8 kWp connected to a 10 kW inverter (SMA STP10000TL-20]. The only difference with the previous system is the solar tracker which is larger and has two stepped motors to assess the tracking (Figure 3).

Figure 3. The CPV system installed in Ajaccio.

The measuring system is composed by:
- A pyrheliometer Kipp & Zonen CHP1 mounted on a SOLYS2 sun tracker measuring DNI;
- A meteorological station Vaisala WTX520 measuring the air temperature, the wind speed and direction, the relative humidity and the atmospheric pressure.

The currents of the two trackers is measured in view to know precisely the tracking angle.

2.2. The data quality control

The measured data must be filtered before to be used for a validation. The data used in this study were measured between 27/06/2017 and 21/06/2019 for Le Bourget du Lac and between 07/04/2016 and 05/05/2019 for Ajaccio.

Three types of control were implemented (Figure 4):
- A control on operational failures or maintenance period on the CPV systems coupled to a control of tracking problems;
- A control on the data acquisition problems: the following filters based on the variables registered values were applied.

- $0 \leq DNI \leq 1000$ (W.m^{-2})
- $0 \leq P_{DC} \leq P_{DC\ CSTC}$ (W), where $P_{DC\ CSTC}$ corresponds to the system's power at CSTC conditions
- $-10 \leq T_{air} \leq 50$ (°C)
- $0 \leq I_{SW} \leq I_{SW\ CSTC}$ (A) and $0 \leq I_{NW} \leq I_{NW\ CSTC}$ (A), where $I_{SW\ CSTC}$ and $I_{NW\ CSTC}$ correspond respectively to the south wing and the north wing currents at CSTC conditions.

- A control of the quality of the data: Mainly to filter data corresponding to high wind velocities and those corresponding to a system partially shaded.
  - $0 \leq v \leq 14$ (m.s^{-1}) where 14 m.s^{-1} is the maximum wind velocity acceptable by the tracker structure during operation.
  - A difference between I_{SW} and I_{NW} less than 10 % relative to the maximum current (to measures realized during partial shading or alignment disequilibrium between the two wings of the tracker).
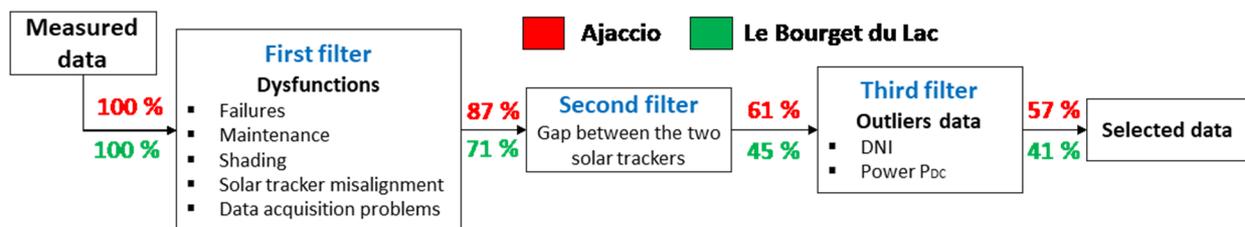

Figure 4. Data control steps.

It appears that the percentage of validated data are relatively small (57% for Ajaccio and 41% for Le Bourget du Lac). Thus 72 469 data of each parameter are available for Le Bourget du lac and 119 008 data for Ajaccio.

3. Choice of DC power models for CPV systems.

3.1. DC power models

The objective of this paper is to elaborate a DC power model for CPV systems using multi-junction PV cells with a simplified utilization so that it could be easily used by photovoltaic system developers and operators.

Thus two important points must be taken into consideration:

- The availability of spectral data is complicated and sometimes impossible; thus, most of the tested models will not use these variables; we will just evaluate the relevance to introduce them.

- The model having to be operational, it must be easy to implement; we will try to determine the effects of the model's simplification on its accuracy.

14

We propose to begin to use models with a reduced number of inputs and to progressively increase the number of data; DNI, T_{air}, AM and v are easily available whereas the spectral distribution of the solar radiation or AOD, PW are rarely available.

Seven models were tested and were divided in two categories (3 models for the first one and 4 models for the second one) according to the forms of the expression inspired from the literature.

- The first category of tested models has an expression (Eq (16)) based on the standard ASTM E 2527-09 [35] which was completed by Garcia-Domingo et al [39] in integrating the solar spectrum effect via the variable SMR.

$$P_{DC} = DNI \cdot \left(a_0 + a_1 \cdot DNI + \sum_{i=2}^{n_v} a_i \cdot y_i\right)$$ (16)

a_0, a_1 and a_i are the model parameters, y_i are the variables which can be T_{air}, v, AM or SMR.

Three models of this category were tested and the expressions are given in <mark>Table 6</mark>:

- o Number 1: using T_{air} and the wind speed v;
- o Number 2: using T_{air}, v and AM (which takes into account more or less the absorption of the solar radiation by the atmosphere);
- o Number 3: using T_{air}, v, and two SMR values $SMR_{\frac{Top}{Middle}}$ and $SMR_{\frac{Middle}{Bottom}}$ taking into account the spectral aspect but rarely available.

- The second category is based on the form of the models introduced by Osterwald [55] and Evans [56] and then used by Fernandez et al [52], the general expression is given by:

$$P_{DC} = P_{DC,ref} \cdot f\left(\frac{DNI}{DNI_{ref}}\right) \cdot \prod_{i=1}^{n_v}(1 + b_i \cdot (x_i - x_{i,ref}))$$ (17)

with $x_{i,ref}$ the value of x_i under the condition $P_{DC}=P_{DC,ref}$ and bi the parameters of the model determined by linear regression.

In this second category of models, the function f of Eq. (17) is based on the works realized by Fernandez et al [57] about the expression of the PV current and voltage at the Maximum Power Point MPP; without variation of the solar spectrum and at constant temperature, Fernandez et al [57] considered that:

- o The current at MPP is proportional to DNI :

$$I_{mpp} = k \cdot DNI$$ (18)

- o The voltage at MPP is the sum of a linear function of the logarithm of DNI ($d_1 \cdot \ln(DNI) + d_3$) and of DNI ($- d_2 \cdot DNI$) based on the single diode model [58]. The voltage increases linearly with ln(DNI) but this increase is slowed by the effect of the serial resistance which is accentuated with the irradiance level (expressed by $- d_2 \cdot DNI$).

$$V_{mpp} = d_1 . \ln(DNI) - d_2 . DNI + d_3 \qquad (19)$$

o The power P_{DC} at MPP is thus obtained by multiplication of V_{mpp} and I_{mpp} (multiplication of Eq. (18) by Eq. (19) :

$$P_{DC}(DNI) = p_1 . DNI + p_2 . DNI^2 + p_3 . DNI . \ln(DNI) \qquad (20)$$

Based on Eq. (20), the function $f\left(\frac{DNI}{DNI_{réf}}\right)$ of Eq. (17) can have two expressions:

o The first one corresponding to Eq. (17) in replacing DNI by $\left(\frac{DNI}{DNI_{ref}}\right)$:

$$f_1\left(\frac{DNI}{DNI_{ref}}\right) = a_{DNI} . \frac{DNI}{DNI_{ref}} + a'_{DNI} . \left(\frac{DNI}{DNI_{ref}}\right)^2 + a''_{DNI} . \frac{DNI}{DNI_{ref}} . \ln\left(\frac{DNI}{DNI_{ref}}\right) \qquad (21)$$

o The second one neglects the variation of the MPP voltage as a function of DNI in Eq. (19) and a simplified expression becomes:

$$f_2\left(\frac{DNI}{DNI_{ref}}\right) = a_{DNI} . \frac{DNI}{DNI_{ref}} \qquad (22)$$

Four models of the second category were tested and the expressions are given in Table 7:

o Number 4: using for $f\left(\frac{DNI}{DNI_{ref}}\right)$ the equation (22) and for variables DNI and T_{air}

o Number 5 : using for $f\left(\frac{DNI}{DNI_{ref}}\right)$ the equation (22) and for variables DNI, T_{air} and AM.

o Number 6: using for $f\left(\frac{DNI}{DNI_{ref}}\right)$ the equation (21) and for variables DNI and T_{air}

o Number 7: using for $f\left(\frac{DNI}{DNI_{ref}}\right)$ the equation (22) and for variables DNI, T_{air}, and SF (which introduces the spectral effects).

Thus, five combinations of models with inputs such as DNI, T_{air}, v and AM in Eq (16) and in Eq (17) coupled with Eq (21) or (22) were tested. Then spectral inputs such as SMR and SF were added in model 3 and 7 in view to evaluate their contribution to the improvement (or not) to the reliability of the model. These models are synthetized in Tables 6 and 7. As we wrote previously, the objective is to increase the complexity of the model and the number of variables and to observe if an improvement appears; it has to be kept in mind that the spectral variables SF and SMR are very limited in many parts of the world and that we are looking for an operational model using easy available data with a good reliability.

Table 6. Models of the first category

Model Number	Inputs - Equations	Expression
1	DNI, T_{air}, v - Eq (16)	$P_{DC} = DNI . (a_0 + a_1 . DNI + a_2 . T_{air} + a_3 . v)$
2	DNI, T_{air}, v, AM - Eq (16)	$P_{DC} = DNI . (a_0 + a_1 . DNI + a_2 . T_{air} + a_3 . v + a_4 . AM)$

16

| 3 | DNI, T_{air}, v, SMR - Eq (16) | $P_{DC} = = DNI.\left(a_0 + a_1.DNI + a_2.T_{air} + a_3.v + a_4.SMR_{\frac{Top}{Middle}} + a_5.SMR_{\frac{Middle}{Bottom}}\right)$ |

<center>Table 7. Models of the second category</center>

Model Number	Inputs - Equations	Expression
4	DNI, Tair - Eq (17) + Eq (22)	$P_{DC} = P_{DC,ref}.\left(p_1.\dfrac{DNI}{DNI_{ref}} + p_2.\dfrac{DNI}{DNI_{ref}}.\left(T_{air} - T_{air,ref}\right)\right)$
5	DNI, Tair, AM - Eq (17) + Eq (22)	$P_{DC} = P_{DC,ref}.\left(a_{DNI}.\dfrac{DNI}{DNI_{ref}}\right).\left(1 + b_{T_{air}}.\left(T_{air} - T_{air,ref}\right)\right).\left(1 + b_{AM}.\left(AM - AM_{ref}\right)\right)$
6	DNI, Tair, AM - Eq (17) + Eq (21)	$P_{DC} = P_{DC,ref}.\left(a_{DNI}.\dfrac{DNI}{DNI_{ref}} + a'_{DNI}.\left(\dfrac{DNI}{DNI_{ref}}\right)^2 + a''_{DNI}.\dfrac{DNI}{DNI_{ref}}.\ln\left(\dfrac{DNI}{DNI_{ref}}\right)\right).\left(1 + b_{T_{air}}.\left(T_{air} - T_{air,ref}\right)\right).\left(1 + b_{AM}.\left(AM - AM_{ref}\right)\right)$
7	DNI, Tair, SF - Eq (17) + Eq (22)	$P_{DC} = P_{DC,ref}.\left(a_{DNI}.\dfrac{DNI}{DNI_{ref}} + a'_{DNI}.\left(\dfrac{DNI}{DNI_{ref}}\right)^2 + a''_{DNI}.\dfrac{DNI}{DNI_{ref}}.\ln\left(\dfrac{DNI}{DNI_{ref}}\right)\right).\left(1 + b_{T_{air}}.\left(T_{air} - T_{air,ref}\right)\right).\left(1 + b_{SF}.\left(SF - SF_{ref}\right)\right)$

The equations of Tables 6 and 7 are linearized and the parameters are computed using the Least Square Method. The linearized form of these equations and the values computed for each site are given in Annex.

3.2. Estimation of spectral indicators SMR and SF

The spectral data SMR and SF are calculated using the SMARTS tool [18] from the variables AM, PW and AOD_{550nm} from the website MODIS [51] (Figure 5).
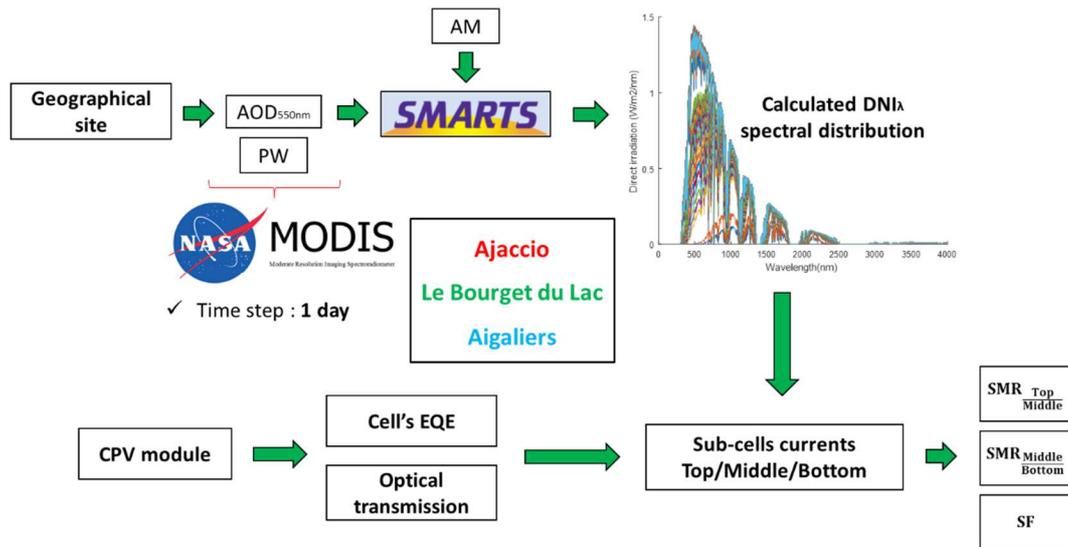
<center>17</center>

Figure 5. Estimation of spectral indicators SF and SMR using SMART [18] from AM, PW and AOD$_{550nm}$

The External Quantum Efficiency (EQE) of the MJSC is obtained from reference [57, 59]. Figure 6 shows the EQE of the GaInP/GaInAs/GaInNAs cells used in the two experimental systems.
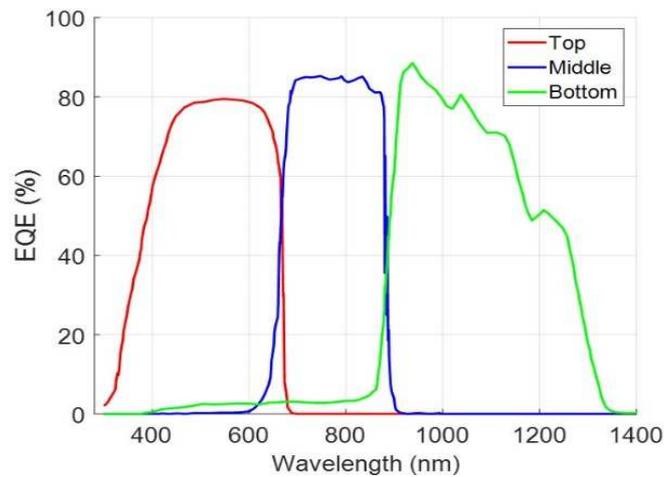

Figure 6. External Quantum Efficiency of the Semprius cell.

The spectral optical transmission of the Primary Optical Element (POE) in silicon on glass (SOG) is presented in Fig. 7 [57].
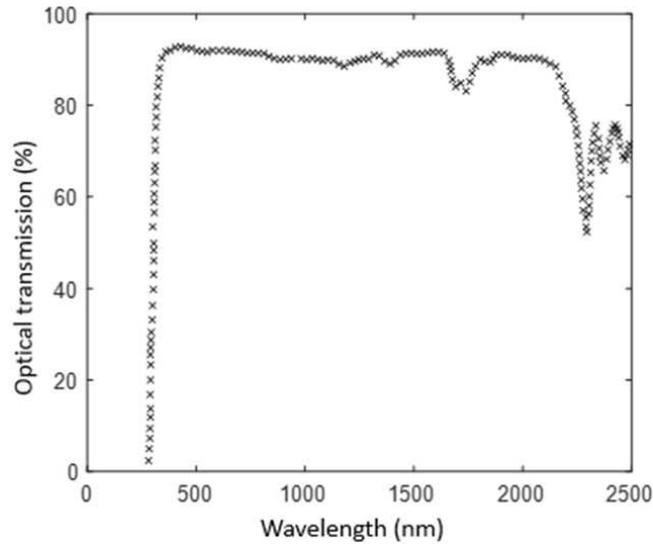
Figure 7. Optical transmission of the Primary Optical Element in silicon on glass.

The average value of SF and SMR are given in Table 8 for the two sites.

Table 8. Average values of the spectral indicators on Ajaccio and Le Bourget du Lac.

Indicator	Ajaccio	Le Bourget du Lac
$\overline{SMR}_{\frac{Top}{Middle}}$	0.81	0.98
$\overline{SMR}_{\frac{Middle}{Bottom}}$	0.90	1.01
$\overline{SF}$	0.91	0.97

It appears clearly that the calculation of SF and SMR values is not a simple task on the one hand and on the other hand, that it necessitates to have PW and AOD550nm data which are difficult to obtain for all sites and with a correct time step.

3. Performances of the models and validation

In this section, firstly one power model will be retained between the seven ones. Then, as the coefficients were independently determined on each site, a second step will consist to use the model established on Ajaccio data and to validate it on the second site.

3.1. Choice of the model

Figure 8 shows the values of the normalized Root Mean Square Error (RMSE) for the seven models applied to the CPV system in Ajaccio and Le Bourget du Lac.

The difference of RMSE between the models is very small whatever the site is. No single coherent model appears clearly.

The introduction of spectral indicators as inputs (models 3 and 7) complicates greatly the model implementation (low availability and difficulty of determination) but too not improves the accuracy of the model. The model 6, inspired by the works of Osterwald [55] and Evans [56] and then used by

Fernandez et al [52], belonging to the second category and using three variables T_{air}, DNI and AM, has the best performances; it uses two frequent measured meteorological data the beam solar irradiance DNI and the ambient temperature T_{air} and the air mass AM easily calculated from the site situation (latitude) and the time. AM influences the attenuation and the diffusion of solar radiation and thus introduces partially the spectral effect of solar radiation. AM being calculated and not measured, the model 6 can be considered as a model with two input data, DNI and T_{air}.

The results obtained from Ajaccio data are less good than from Le Bourget du Lac data; the proximity of the experimental site of the sea (less than 100 meters from the sea and 30 meters above the sea level) influences the solar radiation and its spectral distribution.

In the remainder of this article, only the model 6 is retained for its performance, its reduced number of inputs and the availability of these inputs. However, the values of the coefficients were determined independently for the two sites. The twelve coefficients can be found in Annex; these coefficients have not the same values for the two sites and it appears important to have a unique model applicable to both sites and to make it applicable on several sites independently of the meteorological situation.

Thus, in the following section, the selected model with the coefficients computed with the Ajaccio data will be applied to the second site (the Ajaccio model was chosen as reference because it was trained on a longer period than for the Le Bourget du Lac).
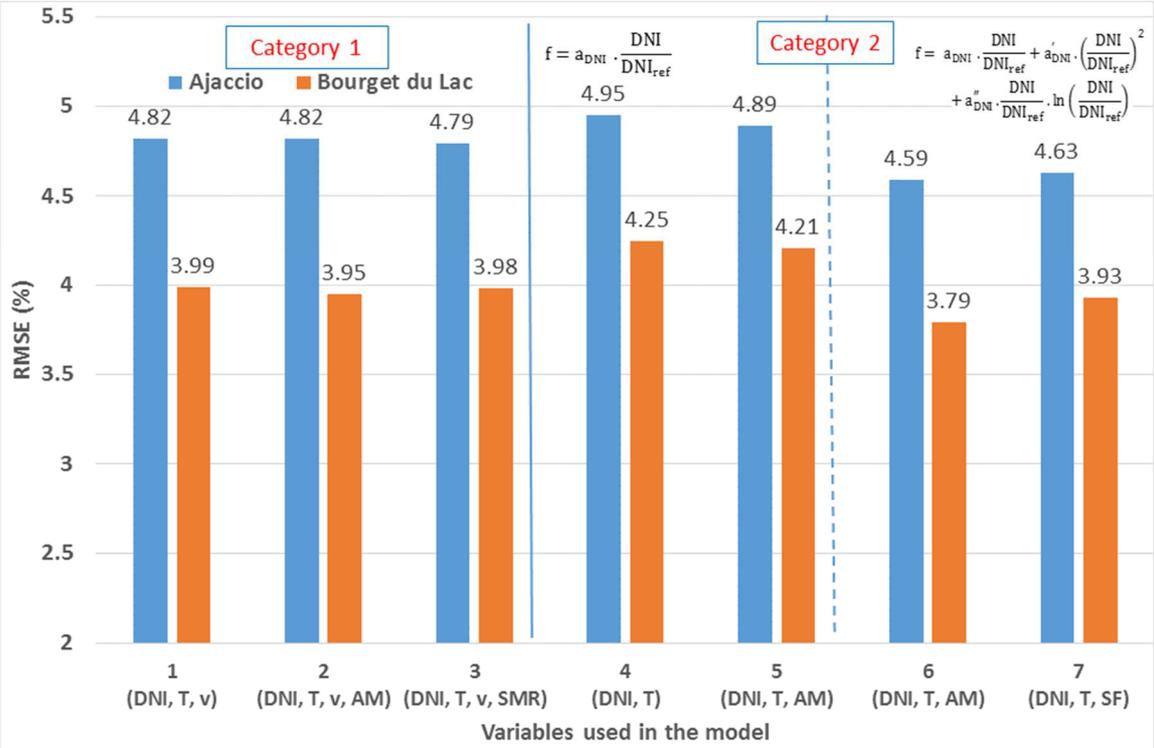

Figure 8. RMSE value for each model applied on the two sites.

3.2. Study of the genericity of the model

The selected model with the coefficients calculated on the Ajaccio data was tested on the data of Le Bourget du Lac and the results are presented in Table 9.

Table 9. Performance of the model with coefficients calculated in Ajaccio tested on the two sites.

Test site	RMSE	MAE
Ajaccio	4.6%	3.9%
Le Bourget du Lac	13.3%	13.0%

The performance of the Ajaccio model applied on the data of Le Bourget du Lac is not satisfying at all because the RMSE was multiplied by 3. It is necessary to determine the causes of the bad performances.

We must keep in mind that the application of the model for a given CPV system necessitates firstly to normalize the electrical power in dividing the produced power by the reference power of the CPV system in Ajaccio; secondly the reduced power calculated for the new CPV system on the second site must be multiplied by the reference power of the new CPV system. The bad performance of our model after its application in the second site can be due to a wrong knowledge of these reference powers on both sites.

Thus, the reference power i.e. the electrical power produced by the CPV system in CSOC (Concentrator Standard Operating Conditions: DNI=900 W.m^{-2}; T_{air} =20°C; v=2 m.s^{-1} and solar spectrum AM1.5D) must be verified experimentally in Ajaccio and Le Bourget du Lac. To do it, we plotted the electrical power versus DNI for various air temperatures (Fig. 9.a) and air mass (Fig. 9.b) for DNI values around CSOC conditions: DNI = (900 ±50) W.m^{-2}, T_{air}= (20±2)°C and AM=1.5±0.1.

(a)

(b)
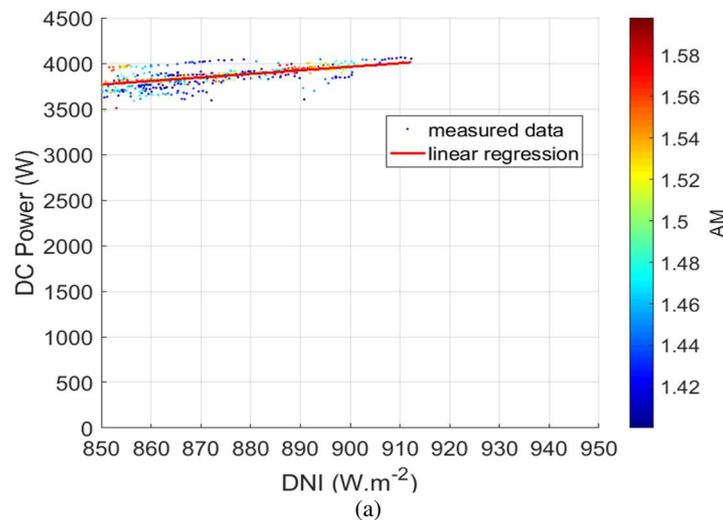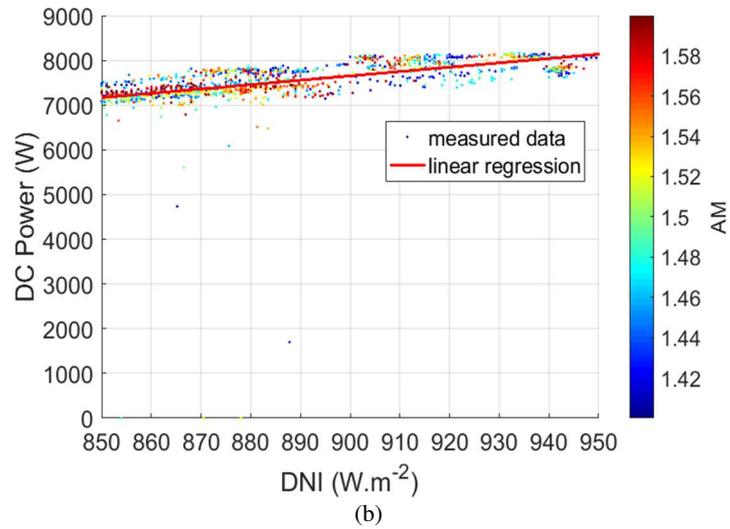
Figure 9. Measured electrical power around CSOC conditions as a function of DNI with a colour scale of AM in Ajaccio (b) and Le Bourget du Lac (a).

The dispersion of the points is mainly due to the variation of the spectral conditions and on the precision of the tracking. Regarding Figure 9, it appears that the average electrical power measured for DNI=900 W.m^{-2} is 7679 W for Ajaccio and 3964 W for Le Bourget du Lac. The manufacturer and experimental electrical power in CSOC are shown and compared in Table 10.

Table 10. Electrical power under CSOC experimentally measured and given by the manufacturer.

	Ajaccio	Le Bourget du Lac
Experimental electrical power under CSOC (Wp)	7679	3964
Electrical power under CSOC given by manufacturer (Wp)	7840	4480
Ratio Experimental/Manufacturer (%)	97.9	88.5

The gap between experimental and "manufacturer" reference power is not negligible mainly for Le Bourget du Lac. Previously, when we applied the model trained on Ajaccio data to the CPV system in Le Bourget du Lac, the normalization was realized in dividing the produced power by the manufacturer CSOC of Ajaccio and the normalized power was then multiplied by the manufacturer CSOC of the CPV system in Le Bourget du Lac (the electrical power of the Ajaccio CPV system was then multiplied by (4480/7840=0.5714). The correction was applied to the model in reducing and then multiplying the model by the experimental CSOC powers (3964/7679=0.5162 i.e. a gap of 9.66% compared with the previous ratio) and the results for the site of Le Bourget du Lac are given in Table 11.

Table 11. Performances of the model before and after the correction by CSOC power.

Using electrical power under CSOC	nRMSE (%)	MAE (%)	MBE (%)
Given by manufacturer	13.3	13.0	13.2
Measured experimentally	4.4	4.0	2.4

We note a high improvement of the performance of the elaborated model and the RMSE and MAE values are of the same order of magnitude for the two sites (RMSE and MAE are equal respectively to 4.6% and 3.9% for Ajaccio and 4.4% and 4.0% for Le Bourget du Lac). These values are in accordance with that found in the literature review; some references gave a RMSE values were between 2.7% and 5.3% and some other ones gave a MAE value between 1.9% and 7.5%. This model can be applied easily without the need of spectral data difficult and costly to obtain and with an accuracy which is of the same order of magnitude as the accuracy of more complex models of the literature.

In view to illustrate the reliability of the model, we plotted experimental and modelled electrical power for some days in Ajaccio and Le Bourget du Lac in Fig. 10.
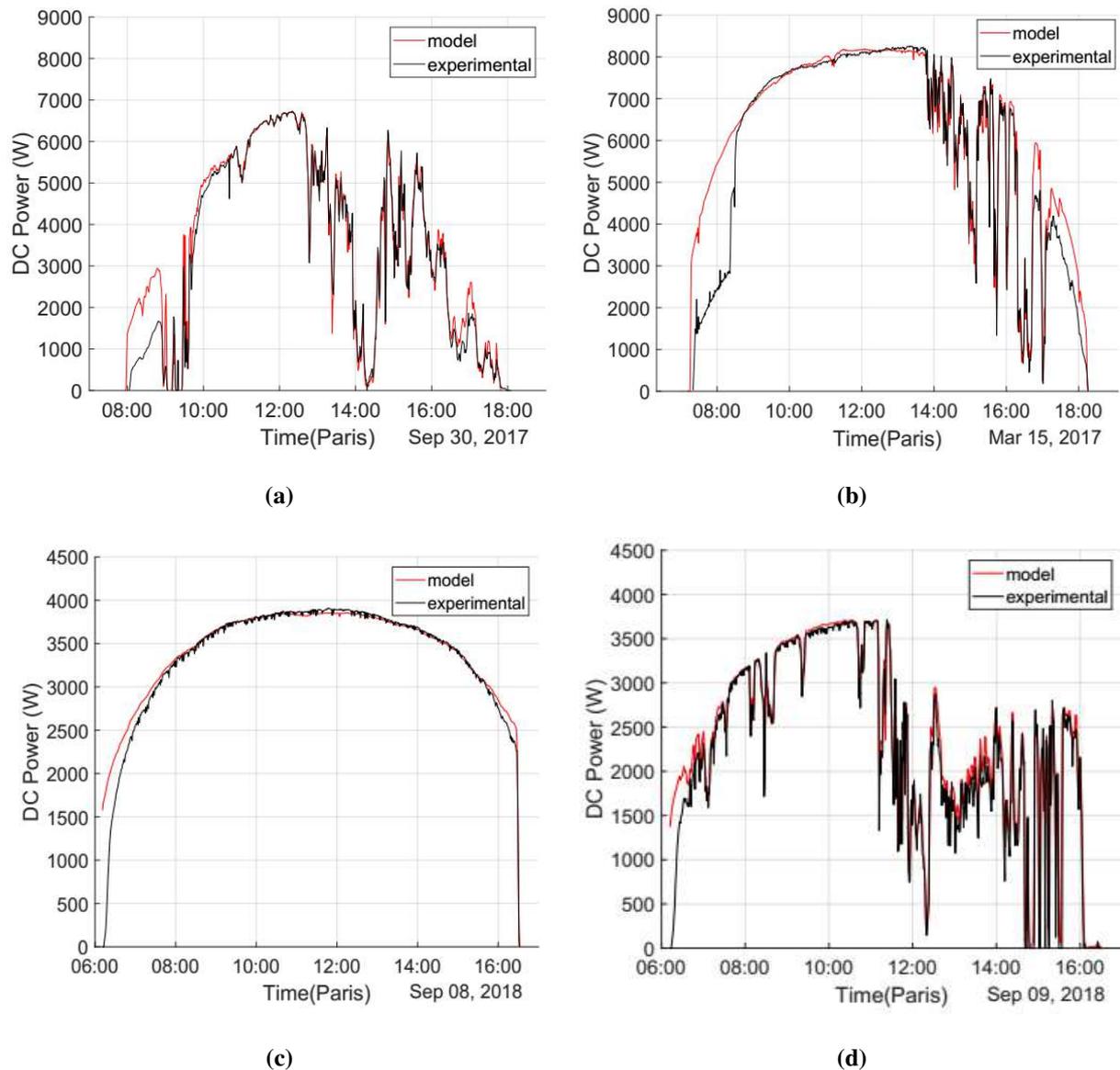
Figure 10. Experimental validation on Ajaccio (a and b) and Le Bourget du Lac (c and d).

The experimental data were not filtered and we can observe some high gaps due to a solar shading (mainly at sunrise hours) or to a misalignment of the tracker.

Conclusions and Perspectives

The objectives of this work were to develop an electrical power model for CPV systems starting from widely available meteorological input data in view to be easily usable by CPV plant operators and investors.

A literature review based on sixteen CPV models was performed: these models are more or less complex and use between two and eleven inputs including rarely measured data such as solar spectrum changing indexes, atmospheric variables like AOD and PW and other system related variables namely the sun tracking accuracy. Some of these models were validated using data measured under controlled

conditions which are far from real operating ones. The most relevant models showed an RMSE between 2.7% and 5.3%.

From this literature review, two categories of model, differing in form, were retained mainly for their simplicity of implementation; in each category, the number of inputs varies but with at least the two more influencing variables DNI and T_{air}. The seven models were validated and tested on two experimental HCPV systems equipped with Semprius SM-U01 modules, composed of micro-concentrators with a concentration ratio equal to 1111 suns and of three junction GaInP/GaInAs/GaInNAs micro-cells. The two HCPV systems have respectively an electrical power in CSOC equal to 7.68 kWp in Ajaccio and 3.96 kWp in Le Bourget du Lac.

The seven tested models showed similar performances and the introduction of spectral indexes did not seem to make an improvement. The most efficient model uses the two main measured meteorological data, beam solar irradiance and ambient temperature, and a calculated parameter, the air mass, introducing partially the spectral effect of solar radiation.

The coefficients of the model were independently calibrated for the two sites and then, the model established on Ajaccio data was validated on the second site data. After a slight correction at the electrical power under CSOC level, the new corrected model showed a RMSE and MAE of 4.6% and 3.9% for Ajaccio and 4.4% and 4.0% for Le Bourget du Lac, values in the same order of magnitude of those found in literature with more complex models.

Several perspectives can be proposed for strengthening and continue this work. First, a study of the spectral effect could be performed. The spectral indicators used in this paper were calculated from daily average values of PW and AOD available on the MODIS website [51]; but their variation during a day can be important and the utilization of hourly data should be interesting provided that these data are available for the study site. Moreover, a more detailed sensitivity study should be performed with particularly an estimation of the influence of the accuracy of the input measures on the CPV power estimation. Then, dependence of the CPV module technology on the results could also be evaluated. A the end, model could be introduced into a PV plant sizing or yield estimating software that do not have, to this day, computing codes adapted to HCPV systems.

References

[1] Hosseinabad ER, Moraga RJ. The evaluation of renewable energy predictive modelling in energy dependency reduction: a system dynamics approach. Int. J. Applied Management Science, 12-1, 1-22.

[2] EurObserv'ER. Photovoltaic Barometer 2019. April 2019. www.eurobserv-er.org.

[3] IRENA (2019), Renewable capacity statistics 2019, International Renewable Energy Agency, Abu Dhabi.

[4] López AL, Andreev VM. Past Experiences and New Challenges of PV Concentrators, G Sala and A Luque, Springer Series in Optical Sciences. 130; 2007. Doi:10.1007/978-3-540-68798-6. ISBN 978-3-540-68796-2

[5] Philipps SP, Bett AW, Horowitz K, Kurtz S. Current status of concentrator photovoltaic (CPV) Technology. Fraunhofer ISE|NREL CPV Report 1.1, December 2015.

[6] Transparency Market Research. Concentrator photovoltaic (CPV) Market - Global Industry Analysis, Size, Share, Growth, Trends, and Forecast, 2016 – 2024; 2016.

[7] Hexa Research. Concentrator Photovoltaic Market Analysis, Market Size, Application Analysis, Regional Outlook, Competitive Strategies and Forecasts, 2016 To 2024. December 2016.

[8] Christiana H, Stuart B. PVEducation - Short-Circuit Current. Available on https://www.pveducation.org/pvcdrom/solar-cell-operation/short-circuit-current. [accessed 16 May 2010].

[9] Fernández EF, Montes-Romero J, de la Casa J, Rodrigo P, Almonacid F. Comparative study of methods for the extraction of concentrator photovoltaic module parameters. Solar Energy 2016;137:413-23.

[10] Segev G, Mittelman G, Kribus A. Equivalent circuit models for triple-junction concentrator solar cells. Solar Energy Materials and Solar Cells 2012;98:57-65.

[11] Nishioka K, Takamoto T, Agui T, Kaneiwa M, Uraoka Y, Fuyuki T. Evaluation of InGaP/InGaAs/Ge Triple-Junction Solar Cell under Concentrated Light by Simulation Program with Integrated Circuit Emphasis. Jpn J Appl Phys 2004;43:882.

[12] Nishioka K, Sueto T, Uchida M, Ota Y. Detailed Analysis of Temperature Characteristics of an InGaP/InGaAs/Ge Triple-Junction Solar Cell. Journal of Elec Materi 2010;39:704-8.

[13] Or AB, Appelbaum J. Estimation of multi-junction solar cell parameters. Progress in Photovoltaics: Research and Applications 2013;21:713-23

[14] Domínguez C, Antón I, Sala G. Multijunction solar cell model for translating I–V characteristics as a function of irradiance, spectrum, and cell temperature. Progress in Photovoltaics: Research and Applications 2010;18:272-84

[15] Fernández EF, Siefer G, Almonacid F, Loureiro AJG, Pérez-Higueras P. A two subcell equivalent solar cell model for III–V triple junction solar cells under spectrum and temperature variations. Solar Energy 2013;92:221-9.

[16] Fernández EF. Modelización y caracterización de células solares iii-v multiunión y de módulos de concentración. PhD thesis, Universidade de Santiago de Compostela, 2012.

[17] Ekins-Daukes NJ, Betts TR, Kemmoku Y, Araki K, Lee H. S, Gottschalg R, Boreland MB, Infield DG, Yamaguchi M. Syracuse - a multi-junction concentrator system computer model. Conference Record of the Thirty-first IEEE Photovoltaic Specialists Conference, 2005.651-4

[18] National Renewable Energy Laboratories (NREL). SMARTS: Simple Model of the Atmospheric Radiative Transfer of Sunshine. 2018. Available on https://www.nrel.gov/grid/solar-resource/smarts.html. [accessed 10 March 2019].

[19] Chan NLA, Young TB, Brindley HE, Ekins-Daukes NJ, Araki K, Kemmoku Y, Yamaguchi M. Validation of energy prediction method for a concentrator photovoltaic module in Toyohashi Japan. Progress in Photovoltaics: Research and Applications 2013; 21:1598-610.

[20] NASA. AERONET Data Download Tool. Available on https://aeronet.gsfc.nasa.gov/cgi-bin/webtool_aod_v3. [accessed 05 April 2010].

[21] Steiner M, Siefer G, Hornung T, Peharz G, Bett AW. YieldOpt, a model to predict the power output and energy yield for concentrating photovoltaic modules. Progress in Photovoltaics: Research and Applications 2015;23:385-97.

[22] Steiner M, Siefer G, Bösch A, Hornung T, Bett AW. Realistic power output modeling of CPV modules. AIP Conference Proceedings 2012;1477:309-12.

[23] Kinsey GS, Hebert P, Barbour KE, Krut DD, Cotal HL, Sherif RA. Concentrator multijunction solar cell characteristics under variable intensity and temperature. Progress in Photovoltaics: Research and Applications 2008;16:503-8.

[24] Kinsey GS, Edmondson KM. Spectral response and energy output of concentrator multijunction solar cells. Progress in Photovoltaics: Research and Applications 2009; 17:279-88.

[25] Kinsey GS, Stone K, Brown J, Garboushian V. Energy prediction of Amonix CPV solar power plants. Progress in Photovoltaics: Research and Applications 2011;19:794-6.

[26] Peharz G, Ferrer Rodríguez JP, Siefer G, Bett AW. A method for using CPV modules as temperature sensors and its application to rating procedures. Solar Energy Materials and Solar Cells 2011;95:2734-44.

[27] Meusel M, Adelhelm R, Dimroth F, Bett AW, Warta W. Spectral mismatch correction and spectrometric characterization of monolithic III–V multi-junction solar cells. Progress in Photovoltaics: Research and Applications 2002;10:243-55.

[28] Peharz G, Siefer G, Bett AW. A simple method for quantifying spectral impacts on multi-junction solar cells. Solar Energy 2009;83:1588-98.

[29] Kratochvil JA, Boyson WE, King DL. Photovoltaic array performance model. 2004. Report No.: SAND2004-3535, 919131. Available on http://www.osti.gov/servlets/purl/919131-sca5ep.

[30] Rodrigo P, Fernández EF, Almonacid F, Pérez-Higueras PJ. Models for the electrical characterization of high concentration photovoltaic cells and modules: A review. Renewable and Sustainable Energy Reviews 2013;26:752-60.

[31] PVSyst. Available on https://www.pvsyst.com/fr/. [accessed 04 April 2019].

[32] Gerstmaier T, Gomez M, Gombert A, Mermoud A, Lejeune T, Dimroth F, Kurtz S, Sala G, Bett AW. Validation of the PVSyst Performance Model for the Concentrix CPV Technology. 7th International Conference On Concentrating Photovoltaic Systems (CPV-7), Las Vegas, Nevada, USA, 2011, pp. 366–369. Doi: 10.1063/1.3658363.

[33] Gerstmaier T, Van Riesen S, Gombert A, Mermoud A, Lejeune T, Duminil E. Software Modeling of FLATCON© CPV Systems. AIP Conference Proceedings 2010; 1277:183-6.

[34] PVSyst. Defining a concentrating system. Available on http://files.pvsyst.com/help/concentrating_definition.htm.

[35] ASTM. ASTM E2527-09, Standard Test Method for Electrical Performance of Concentrator Terrestrial Photovoltaic Modules and Systems Under Natural Sunlight, ASTM International, West Conshohocken, PA, 2009. Doi: 10.1520/E2527-09.

[36] ASTM. ASTM E2527-06, Standard Test Method for Rating Electrical Performance of Concentrator Terrestrial Photovoltaic Modules and Systems Under Natural Sunlight, ASTM International, West Conshohocken, PA, 2006. Doi: 10.1520/E2527-06.

[37] García-Domingo B, Aguilera J, de la Casa J, Fuentes M. Modelling the influence of atmospheric conditions on the outdoor real performance of a CPV (Concentrated Photovoltaic) module. Energy 2014;70:239-50.

[38] Domínguez C, Antón I, Sala G, Askins S. Current-matching estimation for multijunction cells within a CPV module by means of component cells. Progress in Photovoltaics: Research and Applications 2013;21:1478-88.

[39] García-Domingo B, Carmona CJ, Rivera-Rivas AJ, del Jesus MJ, Aguilera J. A differential evolution proposal for estimating the maximum power delivered by CPV modules under real outdoor conditions. Expert Systems with Applications 2015;42:5452-62.

[40] Betts TR, Jardine CN, Gottschalg R, Infield DG, Lane K. Impact of spectral effects on the electrical parameters of multijunction amorphous silicon cells. Proceedings of 3rd World Conference on Photovoltaic Energy Conversion, 2003. 2003; 2: 1756-1759.

[41] Williams SR, Betts TR, Helf T, Gottschalg R, Beyer HG, Infield DG. Modelling long-term module performance based on realistic reporting conditions with consideration to spectral effects. Proceedings of 3rd World Conference on Photovoltaic Energy Conversion, 2003. 2003; 2: 1908-1911.

[42] Moreno Sáez R, Sidrach-de-Cardona M, Mora-López L. Data mining and statistical techniques for characterizing the performance of thin-film photovoltaic modules. Expert Systems with Applications 2013;40:7141-50.

[43] Ishii T, Otani K, Takashima T, Xue Y. Solar spectral influence on the performance of photovoltaic (PV) modules under fine weather and cloudy weather conditions. Progress in Photovoltaics: Research and Applications 2013;21:481-9.

[44] Piliougine M, Elizondo D, Mora-López L, Sidrach-de-Cardona M. Multilayer perceptron applied to the estimation of the influence of the solar spectral distribution on thin-film photovoltaic modules. Applied Energy 2013;112:610-7.

[45] Nofuentes G, García-Domingo B, Muñoz JV, Chenlo F. Analysis of the dependence of the spectral factor of some PV technologies on the solar spectrum distribution. Applied Energy 2014;113:302-9.

[46] Cornaro C, Andreotti A. Influence of Average Photon Energy index on solar irradiance characteristics and outdoor performance of photovoltaic modules. Progress in Photovoltaics: Research and Applications 2013;21:996-1003.

[47] Gueymard. C. Daily spectral effects on concentrating PV solar cells as affected by realistic aerosol optical depth and other atmospheric conditions. Proc. SPIE 7410, Optical Modeling and Measurements for Solar Energy Systems III, 741007 (20 August 2009); doi: 10.1117/12.826071

[48] Husna H. A, Shibata N, Sawano N, Ueno S, Ota Y, Minemoto T, Araki K, Nishioka K. Impact of spectral irradiance distribution and temperature on the outdoor performance of concentrator photovoltaic system. AIP Conference Proceedings 2013; 1556:252-5.

[49] Fernández EF, Almonacid F, Mallick TK, Pérez-Higueras P. Analytical Modelling of High Concentrator Photovoltaic Modules Based on Atmospheric Parameters. International Journal of Photoenergy 2015;2015:8.

[50] Almonacid F, Pérez-Higueras PJ, Fernández EF, Rodrigo P. Relation between the cell temperature of a HCPV module and atmospheric parameters. Solar Energy Materials and Solar Cells 2012;105:322-7.

[51] NASA. MODIS Atmosphere Science Team. MOD08_M3 MODIS/Terra Aerosol Cloud Water Vapor Ozone Monthly L3 Global 1Deg CMG. 2015; available at: http://modaps.nascom.nasa.gov/services/about/products/c6/MOD08_M3.html. [Accessed 06/05/2019].

[52] Fernández EF, Almonacid F, Rodrigo P, Pérez-Higueras P. Model for the prediction of the maximum power of a high concentrator photovoltaic module. Solar Energy 2013;97:12-8.

[53] Almonacid F, Fernandez EF, Mellit A, Kalogirou S. Review of techniques based on artificial neural networks for the electrical characterization of concentrator photovoltaic technology. Renewable and Sustainable Energy Reviews 2017;75:938-53

[54] HeliosLite. Available on https://helioslite.com/index.aspx. [Accessed 27/05/2019].

[55] Osterwald CR. Translation of device performance measurements to reference conditions. Solar Cells 1986;18:269-79.

[56] Evans DL. Simplified method for predicting photovoltaic array output. Solar Energy 1981;27:555-60.

[57] Fernández EF, Almonacid F, Ruiz-Arias JA, Soria-Moya A. Analysis of the spectral variations on the performance of high concentrator photovoltaic modules operating under different real climate conditions. Solar Energy Materials and Solar Cells 2014;127:179-87.

[58] Fernández EF, Ferrer-Rodríguez JP, Almonacid F, Pérez-Higueras P. Current-voltage dynamics of multi-junction CPV modules under different irradiance levels. Solar Energy 2017;155:39-50.

[59] Núñez Júdez R. Contributions to characterization, modeling and design of concentrator photovoltaic systems. PhD dissertation, E.T.S.I. Telecomunicación (UPM), 2016. Available on http://oa.upm.es/43097/.

Linearization of models equations and parameters values

$P_{DC,ref}$ is not in factor in Equation (16), but the parameters given in this annex are divided by the power under CSOC i.e. for Le Bourget du Lac : 4.48 kW and for Ajaccio : 7,84 kW in view to be able to compare the results.

Model 1:

$$P_{DC} = DNI.\,(a_0 + a_1.\,DNI + a_2.\,T_{air} + a_3.\,v)$$

Parameter	le Bourget du lac	Ajaccio	Unity
a_0	0.880	0.990	$m^2.\,kW^{-1}$
a_1	0	0	$W^{-1}.m^4.\,kW^{-1}$
a_2	- 0.001	0.001	$m^2.\,°C^{-1}.kW^{-1}$
a_3	- 0.002	0.002	$m.\,s.\,kW^{-1}$

Model 2 :

$$P_{DC} = DNI.\,(a_0 + a_1.\,DNI + a_2.\,T_{air} + a_3.\,v + a_4.\,AM)$$

Parameter	le Bourget du Lac	Ajaccio	Unity
a_0	0.840	0.980	$m^2.\,kW^{-1}$
a_1	0	0	$W^{-1}.m^4.\,kW^{-1}$
a_2	- 0.001	0.001	$m^2.\,°C^{-1}.kW^{-1}$
a_3	- 0.001	- 0.001	$m.\,s.\,kW^{-1}$
a_4	0.008	0	$m^2.\,kW^{-1}$

Model 3:

$$P_{DC} = = DNI.\left(a_0 + a_1.\,DNI + a_2.\,T_{air} + a_3.\,v + a_4.\,SMR_{\frac{Top}{Middle}} + a_5.\,SMR_{\frac{Middle}{Bottom}}\right)$$

Parameter	le Bourget du Lac	Ajaccio	Unity
a_0	0.851	0.997	$m^2.\,kW^{-1}$
a_1	0	0	$W^{-1}.m^4.\,kW^{-1}$
a_2	- 0.001	0.001	$m^2.\,°C^{-1}.\,kW^{-1}$
a_3	0	0.002	$m.\,s.\,kW^{-1}$
a_4	- 0.119	- 0.016	$m^2.\,kW^{-1}$
a_5	0.098	- 0.005	$m^2.\,kW^{-1}$

Model 4:

$$P_{DC} = P_{DC,ref} \cdot \left(p_1 \cdot \frac{DNI}{DNI_{ref}} + p_2 \cdot \frac{DNI}{DNI_{ref}} \cdot \left(T_{air} - T_{air,ref} \right) \right)$$

Parameter	le Bourget du Lac	Ajaccio	Unity
p_1	0.850	0.970	Without
p_2	- 0.001	0.001	$°C^{-1}$

Model 5:

$$P_{DC} = P_{DC,ref} \cdot \left(a_{DNI} \cdot \frac{DNI}{DNI_{ref}} \right) \cdot \left(1 + b_{T_{air}} \cdot \left(T_{air} - T_{air,ref} \right) \right) \cdot \left(1 + b_{AM} \cdot \left(AM - AM_{ref} \right) \right)$$

$$P_{DC} = P_{DC,ref} \cdot \left(p_1' \cdot \frac{DNI}{DNI_{ref}} + p_2' \cdot \frac{DNI}{DNI_{ref}} \cdot \left(T_{air} - T_{air,ref} \right) + p_3' \cdot \frac{DNI}{DNI_{ref}} \cdot \left(AM - AM_{ref} \right) \right.$$

$$\left. + p_4' \cdot \frac{DNI}{DNI_{ref}} \cdot \left(T_{air} - T_{air,ref} \right) \cdot \left(AM - AM_{ref} \right) \right)$$

Parameter	le Bourget du Lac	Ajaccio	Unity
p_1'	0.851	0.970	Without
p_2'	- 0.001	0.001	$°C^{-1}$
p_3'	- 0.002	- 0.001	Without
p_4'	0.001	0.001	$°C^{-1}$

Model 6:

$$P_{DC} = P_{DC,ref} \cdot \left(a_{DNI} \cdot \frac{DNI}{DNI_{ref}} + a_{DNI}' \cdot \left(\frac{DNI}{DNI_{ref}} \right)^2 + a_{DNI}'' \cdot \frac{DNI}{DNI_{ref}} \cdot \ln \left(\frac{DNI}{DNI_{ref}} \right) \right)$$

$$\cdot \left(1 + b_{T_{air}} \cdot \left(T_{air} - T_{air,ref} \right) \right) \cdot \left(1 + b_{AM} \cdot \left(AM - AM_{ref} \right) \right)$$

$$P_{DC} = P_{DC,ref} \cdot \left(p_1'' \cdot \frac{DNI}{DNI_{ref}} + p_2'' \cdot \left(\frac{DNI}{DNI_{ref}}\right)^2 + p_3'' \cdot \frac{DNI}{DNI_{ref}} \cdot \ln\left(\frac{DNI}{DNI_{ref}}\right) + p_4'' \cdot \frac{DNI}{DNI_{ref}} \cdot (T_{air} \right.$$

$$- T_{air,ref}) + p_5'' \cdot \left(\frac{DNI}{DNI_{ref}}\right)^2 \cdot (T_{air} - T_{air,ref})$$

$$+ p_6'' \cdot \frac{DNI}{DNI_{ref}} \cdot \ln\left(\frac{DNI}{DNI_{ref}}\right) \cdot (T_{air} - T_{air,ref}) + p_7'' \cdot \frac{DNI}{DNI_{ref}} \cdot (AM - AM_{ref})$$

$$+ p_8'' \cdot \left(\frac{DNI}{DNI_{ref}}\right)^2 \cdot (AM - AM_{ref}) + p_9'' \cdot \frac{DNI}{DNI_{ref}} \cdot \ln\left(\frac{DNI}{DNI_{ref}}\right) \cdot (AM - AM_{ref})$$

$$+ p_{10}'' \cdot \frac{DNI}{DNI_{ref}} \cdot (T_{air} - T_{air,ref}) \cdot (AM - AM_{ref}) + p_{11}'' \cdot \left(\frac{DNI}{DNI_{ref}}\right)^2 \cdot (T_{air}$$

$$- T_{air,ref}) \cdot (AM - AM_{ref}) + p_{12}'' \cdot \frac{DNI}{DNI_{ref}} \cdot \ln\left(\frac{DNI}{DNI_{ref}}\right) \cdot (T_{air}$$

$$\left. - T_{air,ref}) \cdot (AM - AM_{ref}) \right)$$

Parameter	le Bourget du Lac	Ajaccio	Unity
p_1''	0.940	1.280	Without
p_2''	- 0.070	- 0.310	Without
p_3''	0.160	0.290	Without
p_4''	0.014	0.030	°C^{-1}
p_5''	- 0.015	- 0.030	°C^{-1}
p_6''	0.009	0.020	°C^{-1}
p_7''	- 0.530	- 0.090	Without
p_8''	0.600	0.090	Without
p_9''	- 0.280	- 0.060	Without
p_{10}''	0	- 0.010	°C^{-1}
p_{11}''	- 0,001	0,010	°C^{-1}
p_{12}''	- 0,002	0,003	°C^{-1}

Model 7:

$$P_{DC} = P_{DC,ref} \cdot \left(a_{DNI} \cdot \frac{DNI}{DNI_{ref}} + a_{DNI}' \cdot \left(\frac{DNI}{DNI_{ref}}\right)^2 + a_{DNI}'' \cdot \frac{DNI}{DNI_{ref}} \cdot \ln\left(\frac{DNI}{DNI_{ref}}\right) \right)$$

$$\cdot \left(1 + b_{T_{air}} \cdot (T_{air} - T_{air,ref})\right) \cdot \left(1 + b_{SF} \cdot (SF - SF_{ref})\right)$$

$$P_{DC} = P_{DC,ref} \cdot \left(w_1 \cdot \frac{DNI}{DNI_{ref}} + w_2 \cdot \left(\frac{DNI}{DNI_{ref}}\right)^2 + w_3 \cdot \frac{DNI}{DNI_{ref}} \cdot \ln\left(\frac{DNI}{DNI_{ref}}\right) + w_4 \cdot \frac{DNI}{DNI_{ref}} \cdot (T_{air} - T_{air,ref}) \right.$$

$$+ w_5 \cdot \left(\frac{DNI}{DNI_{ref}}\right)^2 \cdot (T_{air} - T_{air,ref}) + w_6 \cdot \frac{DNI}{DNI_{ref}} \cdot \ln\left(\frac{DNI}{DNI_{ref}}\right) \cdot (T_{air} - T_{air,ref})$$

$$+ w_7 \cdot \frac{DNI}{DNI_{ref}} \cdot (SF - SF_{ref}) + w_8 \cdot \left(\frac{DNI}{DNI_{ref}}\right)^2 \cdot (SF - SF_{ref}) + w_9 \cdot \frac{DNI}{DNI_{ref}} \cdot \ln\left(\frac{DNI}{DNI_{ref}}\right) \cdot (SF - SF_{ref})$$

$$+ w_{10} \cdot \frac{DNI}{DNI_{ref}} \cdot (T_{air} - T_{air,ref}) \cdot (SF - SF_{ref}) + w_{11} \cdot \left(\frac{DNI}{DNI_{ref}}\right)^2 \cdot (T_{air} - T_{air,ref}) \cdot (SF - SF_{ref})$$

$$\left. + w_{12} \cdot \frac{DNI}{DNI_{ref}} \cdot \ln\left(\frac{DNI}{DNI_{ref}}\right) \cdot (T_{air} - T_{air,ref}) \cdot (SF - SF_{ref}) \right)$$

Parameter	le Bourget du Lac	Ajaccio	Unity
w_1	1.151	1.277	Without
w_2	- 0.282	- 0.302	Without
w_3	0.292	0.295	Without
w_4	0.009	0.038	$°C^{-1}$
w_5	- 0.011	- 0.039	$°C^{-1}$
w_6	- 0.004	0.019	$°C^{-1}$
w_7	- 0.990	0.027	Without
w_8	1.229	- 0.029	Without
w_9	- 1.207	0.017	Without
w_{10}	- 0.080	0.002	$°C^{-1}$
w_{11}	0.063	- 0.002	$°C^{-1}$
w_{12}	- 0.064	0.001	$°C^{-1}$